Available online at www.sciencedirect.com
SCIENCE DIRECT
Cryogenics 46 (2006) 658–665
Cryogenics
www.elsevier.com/locate/cryogenics

Multi-dimensional flow effects in pulse tube refrigerators

J.S. Cha [a], S.M. Ghiaasiaan [a,*], P.V. Desai [a], J.P. Harvey [b], C.S. Kirkconnell [b]

[a] G.W. Woodruff School of Mechanical Engineering, Georgia Institute of Technology, Atlanta, GA 30332, USA
[b] Raytheon Electronic Systems El Segundo, CA 90245-0902, USA

Received 15 September 2005; received in revised form 6 March 2006; accepted 10 March 2006

Abstract

Pulse tube cryocoolers are often modeled as one-dimensional flow fields. We examine the adequacy of this assumption in this study. Two entire inertance tube pulse tube refrigerator (ITPTR) systems operating under a variety of thermal boundary conditions are modeled using a computational fluid dynamics (CFD) code. Each simulated ITPTRs includes a compressor, an after cooler, a regenerator, a pulse tube, cold and hot heat exchangers, an inertance tube, and a reservoir, and the simulations represent fully coupled systems operating in steady-periodic mode. The objectives are to ascertain the suitability of CFD methods for ITPTRs, and examine the extent of multi-dimensional flow effects in various ITPTR components. The results confirm that CFD simulations are capable of elucidating complex periodic processes in ITPTRs. The results also show that one-dimensional modeling is appropriate only when all the components in the system have large length-to-diameter (L/D) ratios. Significant multi-dimensional flow effects occur at the vicinity of component-to-component junctions, and secondary-flow recirculation patterns develop when one or more components have relatively small L/D ratios. Parameters in need of experimental measurement are discussed.

Keywords: Pulse tube (E); Regenerators (E); Space cryogenics (F); Flow visualization (D)

1. Introduction

The design of pulse tube refrigerator (PTR) systems has advanced incessantly since the invention of basic PTR [1], leading to improvements in their performance and lower achievable refrigeration temperatures. The major design variations introduced thus far include the orifice pulse tube refrigerator (OPTR) [2], double inlet OPTR [3], the modified OPTR [4], the multi-pass OPTR [5], and most recently the inertance tube pulse tube refrigerator (ITPTR) [6]. The exact nature of the physical phenomena underlying the operation of PTRs is not well-understood, however [7,8]. A fundamental difficulty in all PTRs is that their working fluid compression and expansion processes are not well-defined, and poorly-understood thermal relaxation and phase-lag phenomena dominate their operation. Crucial among these is the phase angle between pressure and mass flow. This phase angle is influenced by the wave resonance phenomena in BPTRs, and is adjusted by orifices and/or valves in various OPTR designs. In an ITPTR, the orifice valve of the simple OPTR is replaced by an Inertance tube that, with proper design, can cause an optimal phase lag between pressure and mass flow rate in the pulse tube.

Thermodynamic models have been used for the analysis of PTRs [9,10]. These models, although simple and convenient to use, do not adequately consider the flow and heat transfer details. Computational models have recently been developed for the simulation of the regenerator, or the entire PTR [12–14]. The sage computer package [11] models an entire PTR assuming 1D flow, and can optimize a system against a user-selected geometric parameter. The numerical model of [12] is also 1D and appears to simulate an entire PTR system. Simulation of complete PTRs system using CFD software packages has also been recently published. Hozumi et al. [13] performed axi-symmetric and 3D simulations of BPTRs and OPTRs, with an interest

* Corresponding author. Tel.: +1 404 894 3746; fax: +1 404 894 8496.
E-mail address: seyed.ghiaasiaan@me.gatech.edu (S.M. Ghiaasiaan).

0011-2275/$ - see front matter © 2006 Elsevier Ltd. All rights reserved.
doi:10.1016/j.cryogenics.2006.03.001

Nomenclature

$\overline{\overline{C}}$	inertial drag coefficient tensors (m^{-1})
h	enthalpy (J/kg)
j	superficial velocity (m/s)
k	thermal conductivity (W/m K)
p	pressure (N/m^2)
T	temperature (k)
t	time (s)
v	intrinsic velocity (m/s)
ω	angular frequency (rad/s)
x	piston displacement (m)
x_a	piston displacement amplitude (m)

Greek letters

$\overline{\overline{\beta}}$	permeability tensors (m^2)
ε	porosity
μ	absolute viscosity (kg/m s)
ρ	density (kg/m^3)
$\overline{\overline{\tau}}$	stress tensors (N/m^2)

Subscripts

f	fluid
r	radial coordinate
s	solid
x	axial coordinate

in the effects of gravity and orientation on system performance. Flake and Razani [14] conducted an axi-symmetric analysis of a BPTR and an OPTR, using the Fluent® [15] commercial CFD package, and indicated the occurrence of recirculation patterns and streaming effects in their simulated pulse tube.

A PTR is a multifaceted flow loop that consists of components in which complex solid fluid thermal interactions take place. Some of the components can best be modeled as porous media. The system operates under periodic flow, furthermore. CFD simulation of a PTR system is not straightforward, and can produce meaningful results only when reasonably accurate closure relations representing the fluid–solid interactions are applied.

In this paper, we report on CFD simulations addressing the steady-periodic operation of two ITPTR systems. The objectives of the study were to assess the feasibility of CFD simulation of ITPTRs, examine the extent and significance of multi-dimensional flow effects in these systems, and identify and discuss the poorly-understood parameters that are needed for the closure of conservation equations that are numerically solved by the CFD codes.

2. Simulated systems

Two ITPTR systems, referred to as MOD1 and MOD2 hereafter, were simulated using the Fluent [15] code. A schematic of the ITPTR system is shown in Fig. 1, and the geometric dimensions of all the components are listed in Table 1. The system designated as MOD1 is in fact identical to the experimental test apparatus of Kirkconnell et al. [16,17] and Harvey et al. [18], with the exception that MOD1 includes an inertance tube (IT) instead of an orifice. The MOD2 system is similar to MOD1, except that the regenerator, pulse tube, and inertance tube components of MOD2 have different geometric dimensions than MOD1.

Three different operational modes were simulated for MOD1 and MOD2 each, as summarized in Table 2. The three cases for each system address operation with an adiabatic cold end heat exchanger (CHX) (i.e., zero cooling load), a specified CHX cooling load, and a known CHX

Table 1
Dimensions of the simulated systems according to Fig. 1

Components	MOD1		MOD2	
	Radius (m)	Length (m)	Radius (m)	Length (m)
A (Compressor)	9.54E−03	7.50E−03	9.54E−03	7.50E−03
B (Transfer line)	1.55E−03	1.01E−01	1.55E−03	1.01E−01
C (WHX1)	4.00E−03	2.00E−02	4.00E−03	2.00E−02
D (Regenerator)	4.00E−03	5.80E−02	1.00E−02	2.50E−02
E (CHX)	3.00E−03	5.70E−03	3.00E−03	5.70E−03
F (Pulse tube)	2.50E−03	6.00E−02	7.50E−03	3.00E−02
G (WHX2)	4.00E−03	1.00E−02	4.00E−03	1.00E−02
H (Inertance Tube)	4.25E−04	6.84E−01	5.96E−04	1.07E+00
I (Surge volume)	1.30E−02	1.30E−01	1.30E−02	1.30E−01

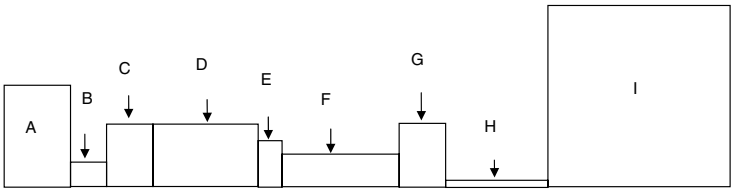

Fig. 1. The Simulated ITPTR System.

Table 2
Boundary conditions for the simulations

Components	MOD1			MOD2		
	Case 1	Case 2	Case 3	Case 4	Case 5	Case 6
WHX1 wall temperature (K)	293	293	293	293	293	293
CHX wall conditions	Adiabatic	1 W load	150 K	Adiabatic	1 W load	282 K
WHX2 wall temperature (K)	293	293	293	293	293	293
CHX load (W)	0	1	**6.39**[a]	0	1	**2.57**[a]
CHX surface temperature (K)	**87**[a]	**100**[a]	150	**278**[a]	**280**[a]	282

[a] These values were obtained from simulations.

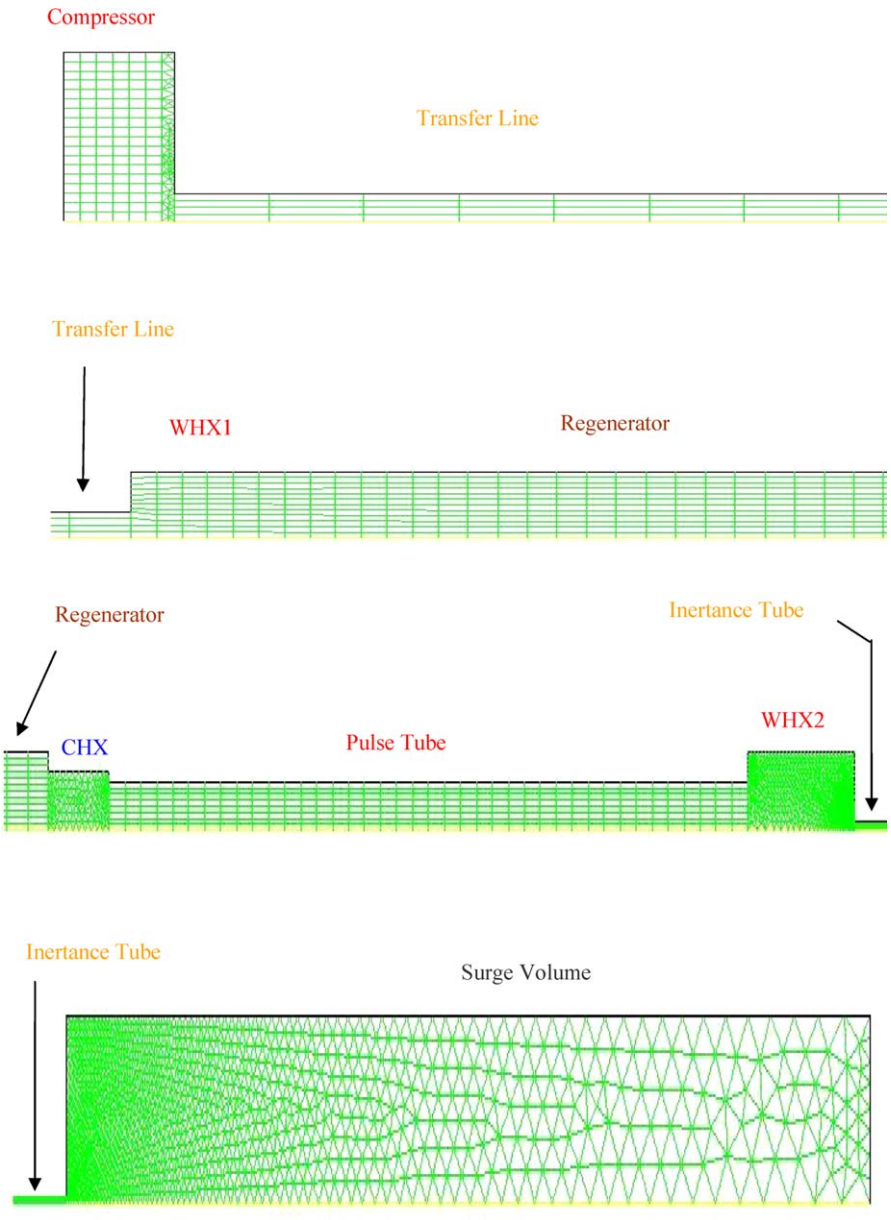

Fig. 2. Nodalization of the MOD1 simulated system.

surface temperature. The boundary conditions depicted in Table 2 were the only parameters that were provided to the forthcoming CFD simulations. The entries that are shown in bold characters, furthermore, are calculated results from simulations. All other system boundaries were assumed to be adiabatic.

3. CFD models

The commercial CFD code Fluent® [15] was used. Given the assumed cylindrical and linear alignment of the simulated ITPTR systems, axi-symmetric, two-dimensional flow was assumed. Using a simple user defined function, the piston head motion was modeled as

$$X = X_a \sin(\omega t) \tag{1}$$

where $X_a = 4.511 \times 10^{-3}$ m, $\omega = 213.62$ rad/s, and the time increment of 7.3529×10^{-4} s were assumed.

Fluent is equipped with a dynamic meshing function that can create deformable mesh volumes. This function was utilized for modeling the compressor. Detailed nodalization of all components was performed, whereby regions deemed more sensitive, such as the vicinity of component-to-component junctions, were represented by finer mesh than others. The exact number of nodes varied from case to case. The MOD1 system was thus represented by 4067–4198 nodes for Cases 1–3, and the MOD2 systems was represented by a total of 4347–4385 nodes for Cases 4–6. Numerical tests, to be discussed in the Appendix, showed that these numbers of nodes lead to results that were reasonably grid number-independent. Fig. 2 depicts the nodalization of the simulated system MOD1.

The mass, momentum and energy equations solved by Fluent for the forthcoming simulations are, respectively:

$$\frac{\partial \rho_f}{\partial t} + \frac{1}{r}\frac{\partial}{\partial r}[r\rho_f v_r] + \frac{\partial}{\partial x}[\rho_f v_x] = 0 \tag{2}$$

$$\frac{\partial}{\partial t}[\rho_f \vec{v}] + \nabla \cdot [\rho_f \vec{v}\vec{v}] = -\nabla p + \nabla \cdot [\bar{\bar{\tau}}] \tag{3}$$

$$\frac{\partial}{\partial t}[\rho_f E] + \nabla \cdot [\vec{v}(\rho_f E + p)] = \nabla \cdot [k_f \nabla T + (\bar{\bar{\tau}} \cdot \vec{v})] \tag{4}$$

where

$$E = h - \frac{p}{\rho} + \frac{v^2}{2} \tag{5}$$

All properties represent the properties of the working fluid helium. The above equations apply to all components, except for CHX, WHX1, WHX2 and the regenerator. The latter four components are modeled as porous media, assuming that there is local thermodynamic equilibrium between the fluid and the solid structure in these components. The mass, momentum, and energy equations in the latter four components are:

$$\frac{\partial}{\partial t}[\varepsilon\rho_f] + \frac{1}{r}\frac{\partial}{\partial r}[\varepsilon r \rho_f v_r] + \frac{\partial}{\partial x}[\varepsilon \rho_f v_x] = 0 \tag{6}$$

$$\frac{\partial}{\partial t}[\varepsilon\rho_f \vec{v}] + \nabla \cdot [\varepsilon\rho_f \vec{v}\vec{v}] = -\varepsilon\nabla p + \nabla \cdot [\varepsilon\bar{\bar{\tau}}] - \left[\mu \bar{\bar{\beta}}^{-1} \cdot \vec{j} + \frac{1}{2}\bar{\bar{C}}\rho_f \cdot |\vec{j}|\vec{j}\right] \tag{7}$$

$$\frac{\partial}{\partial t}[\varepsilon\rho_f E_f + (1-\varepsilon)\rho_s E_s] + \nabla \cdot [\vec{v}(\rho_f E_f + p)] = \nabla \cdot \left[(\varepsilon k_f + (1-\varepsilon)k_s)\nabla T + (\varepsilon\bar{\bar{\tau}} \cdot \vec{v})\right] \tag{8}$$

where $\varepsilon = 0.69$, $\bar{\bar{\beta}} = 1.06 \times 10^{-10}$ m^2, and $\bar{\bar{C}} = 7.609 \times 10^4$ m^{-1} were assumed. These parameters are based on the experiments of Harvey [19] for axial flow through a randomly packed stack of 325 mesh stainless steel screens.

For simplicity, all the simulations were done as transient processes, starting with an initial system temperature of 300 K for Cases 1–3, and 293 K for Cases 4–6. Simulations were continued until steady-periodic state was obtained. The criterion for steady periodic condition was that the cycle-average temperature of the cold end heat exchanger (CHX) would reach a steady state.

4. Results and discussion

4.1. General observations

The variations of the cycle-average temperature of the CHX surface are depicted in Fig. 3 for Cases 1, 2, 4 and 5, and show the development of steady-periodic states. For Cases 3 and 6, where a constant CHX surface temperature was imposed, steady periodic state can be easily recognized by plotting the temporal variation of the total rate

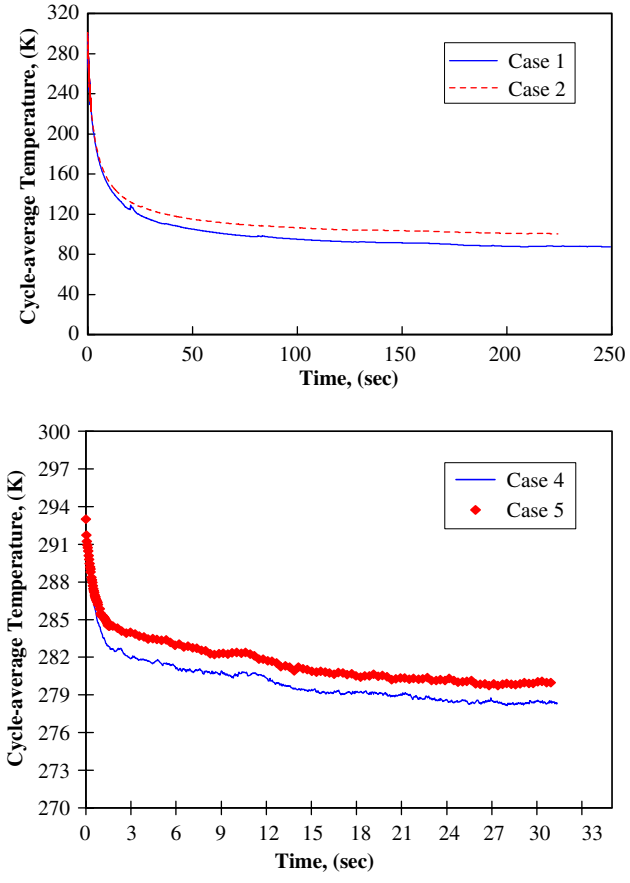

Fig. 3. Temporal variations of cycle-average CHX surface temperature for simulation cases with a cooling load of 1 W.

of heat absorbed by the system through CHX (cooling load).

The axial distributions of cross-section and cycle-averaged temperature for Cases 1–3, under steady-periodic state, are displayed in Fig. 4. Significant temperature gradients are predicted in the regenerator and the pulse tube. These profiles are evidently consistent with the known trends in data. The overall performances of the simulated systems are represented by the calculated CHX temperatures depicted in Table 2. Besides well-expected trends (e.g., higher cold tip temperatures with a cooling load of 1 W, in comparison with cases with zero cooling load), an interesting observation is that simulation Cases 1–3 perform better than Cases 4–6. The MOD1 system being made of modules with large L/D, is evidently superior to the MOD2 system.

4.2. Multi-dimensional effects

Intuition suggests that multi-dimensional flow effects become more significant as a component's L/D ratio is reduced, and that the most significant multi-dimensional effects should occur at the vicinity of component-to-component junctions. Details of the simulation flow fields fully support these observations. Figs. 5 and 6 depict the cycle-average temperature contours for Cases 2 and 5, respectively. The multi-dimensional effects in all simulations dealing with MOD1 system were relatively minor. Significant

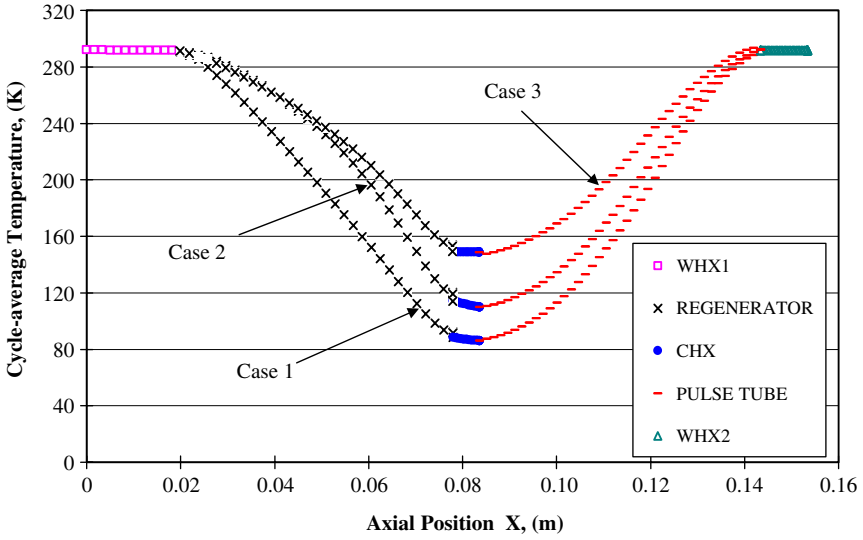

Fig. 4. Axial distribution of cross-section and cycle-averaged temperature distributions under steady periodic for Cases 1–3 (MOD1 system).

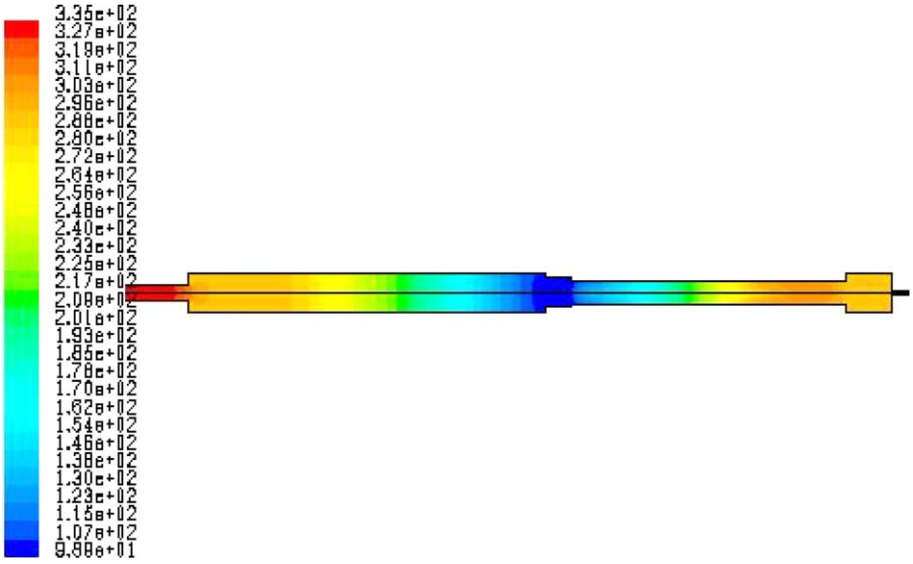

Fig. 5. Steady-periodic cycle-average temperature contours for simulation Case 2.

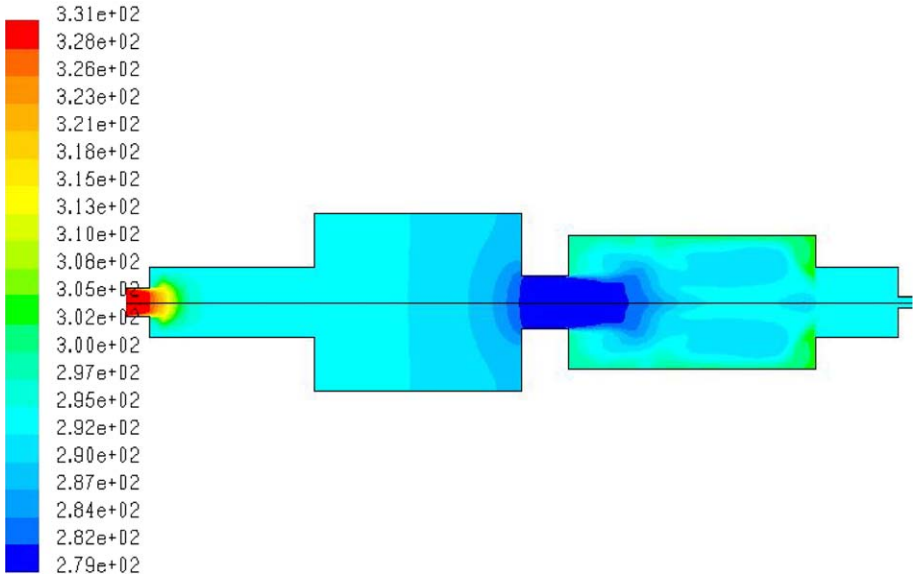

Fig. 6. Steady-periodic cycle-average temperature contours for simulation Case 5.

multi-dimensional effects occurred in MOD2 system, however. Typical snapshots of the fluid velocity and temperature distributions representing the regenerator and the pulse tube of the MOD2 system are depicted in Figs. 7 and 8, respectively. The two figures are associated with Case 4, under steady-periodic conditions. For both components, strong multi-dimensional effects occur near their two ends. The secondary flows, in the form of recirculation patterns are predicted for the pulse tube. The multi-dimensional flows undoubtedly impact pressure drop, dissipation and heat transfer processes, in particular in the regenerator. The multitude of recirculation pattern in the pulse tube cause undesirable mixing in the thermally stratified fluid, and is at least partially responsible for the poor overall performance of the MOD2 system.

The occurrence of periodic and multi-dimensional flows indicates the need for careful experimental measurement and correlation of hydrodynamic parameters (e.g., the permeability and Forchheimer coefficients) for the regenerator. Most regenerator fillers are morphologically anisotropic, and experimental measurements of their hydrodynamic parameters are needed at least in two (axial and radial) directions. The periodicity of the flow field should also be considered in the experimental measurement

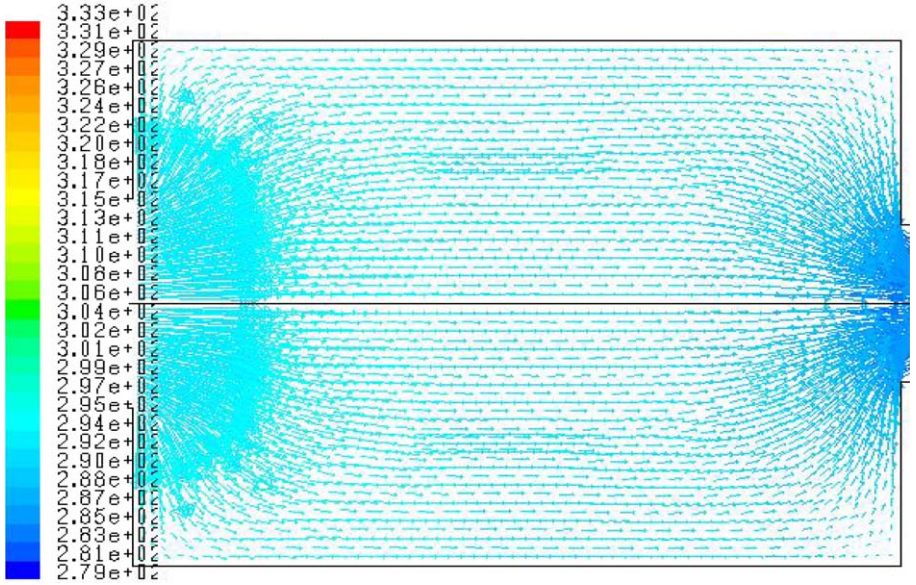

Fig. 7. Snapshot of velocity vectors and temperatures (K) in the regenerator of MOD2 system during the simulation Case 4.

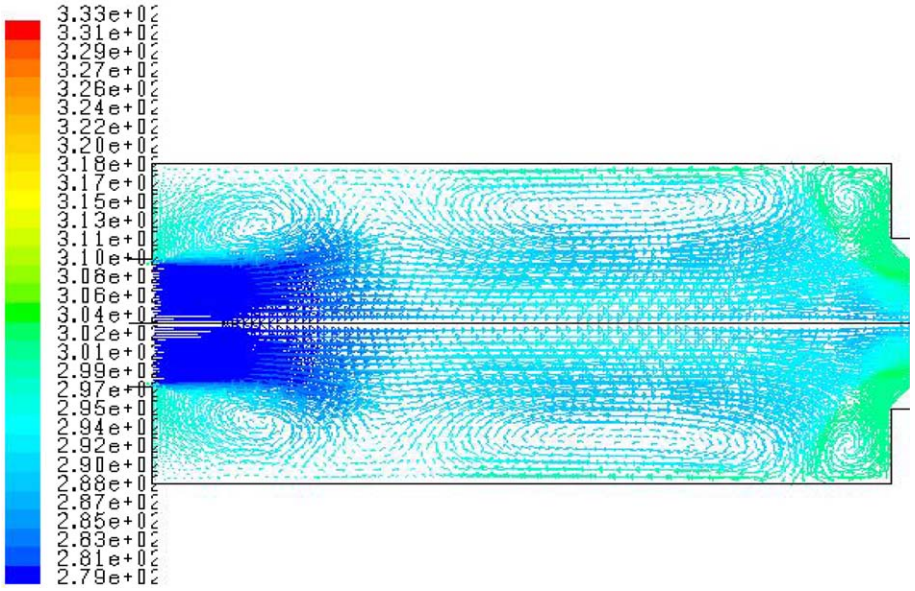

Fig. 8. Snapshot of velocity vectors and temperatures (K) in the pulse tube of MOD2 system during the simulation Case 4.

of the latter parameters. Periodic laminar flow in channels and tubes has been investigated extensively in the past [20–25]. Except for some investigations dealing with the axial dispersion in packed beds [25–28], little is known about the hydrodynamics of porous media in periodic flow. The common approach in cryocooler modeling is to use constant cycle-average coefficients for one-dimensional flow [12,29], with little justification.

The aforementioned observations were all based on numerical simulations, and evidently need to be verified by comparison with experiments. Relevant experiments for ITPTRs are not available at this time, however. An experimental program is underway at Georgia Institute of Technology aimed at the measurement and correlation of axial and radial permeability and Forchheimer coefficients for some of the most widely-used regenerator filler configurations, under steady state, as well as pulsating and periodic flows.

5. Conclusions

Two entire ITPTR systems, operating in steady periodic state under a variety of boundary conditions, were numerically simulated, using the CFD package Fluent [15]. The objectives were to demonstrate the feasibility of CFD simulation of PTRs, and to examine the multi-dimensional flow and heat transfer effects. CFD simulations successfully predicted all the expected trends. They also showed that a 1D analysis can be adequate only when all the components of the ITPTR have large length-to-diameter ratios. Significant multi-dimensional effects and working fluid recirculation occur when one or more components have relatively small L/D ratios. The recirculation patterns deteriorate the overall performance of the system.

Acknowledgements

The authors acknowledge gratefully the financial and technical support for this work by Raytheon Company.

Appendix. Convergence and grid-independence

Numerical tests were performed in order to ascertain that the simulation results were grid number-independent, and that the basic conservation laws were adhered to in the simulations.

Typical test results are displayed in Fig. A.1, where the transient variations of cycle-average temperature of the Component CHX associated with Case 2 in Table 2, are plotted, with only one difference. The cooling load on the component CHX was set at 1.91 W. The predicted results are shown for three simulations. The three simulations use a total of 4274, 4958, and 6296 nodes for the entire system. It can be noted that there is little difference between the three simulations as the steady-state is approached. The predictions of the three simulations for other system parameters were similarly close, confirming that the results are reasonably grid number-independent when a total of about 4200 nodes is used.

Our tests also showed that the numerical error could be reduced to a negligible level using the second-order upwind differencing scheme. For the aforementioned simulations dealing with grid number – independence, with scaled residual error limits of 10^{-5} for mass and velocity, and 10^{-7} for energy, mass conservation during the entire simulation time could be satisfied within less than 0.4%. Most of the simulations displayed in this paper were obtained using a scaled residual error of 10^{-3} for mass and velocity, and 10^{-6} for energy, however. For these simulations the overall

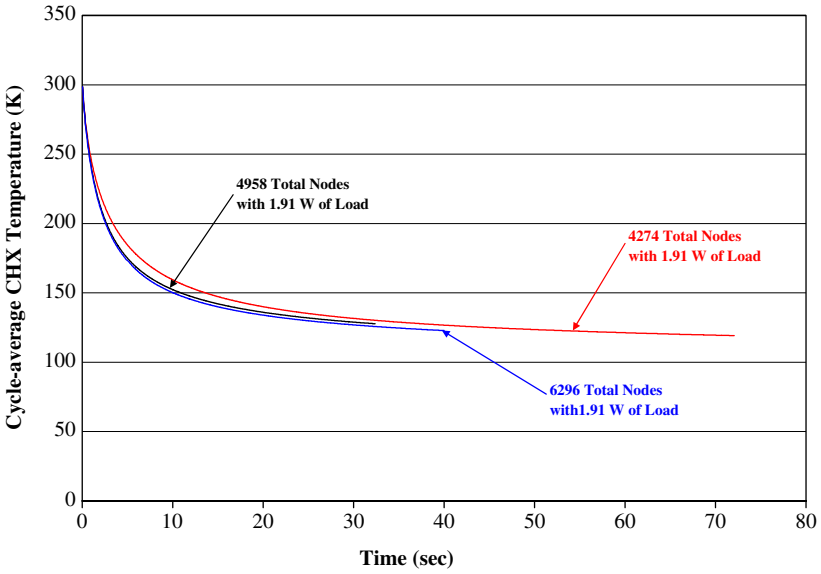

Fig. A.1. The effect of the total number of grids on the cycle-average temperature of component CHX2 for Case 2, modified to have a cooling load of 1.91 W.

error in mass conservation for the entire system was typically less than 1.7%, but reached the maximum value of 4.7% for Case 2 in Table 2.

References

[1] Gifford W, Longsworth R. Pulse-tube refrigeration. Trans ASME, J Eng Ind (series B) 1964;86:264–8.

[2] Mikulin E, Tarasov A, Shrebyonock M. Low-temperature expansion pulse tubes. Adv Cryogen Eng 29:629–37.

[3] Zhu S, Wu P, Chen Z. A single stage double inlet pulse tube refrigerator capable of reaching 42 K. ICEC 13 Proc Cryogenics 1990;30:256–61.

[4] Wang C, Wu P, Chen Z. Modified orifice pulse tube refrigerator without a reservoir. Cryogenics 1994;34:31–6.

[5] Cai J, Wang J, Zhu W, Zhou Y. Experimental analysis of double-inlet principle in pulse tube refrigerator. Cryogenics 1993;33:522–5.

[6] Zhu S, Zhou S, Yoshimura N, Matsubara Y. Phase shift effect of the long neck tube for the pulse tube refrigerator. In: Proceedings of the 9th international cryocoolers conference, June 1996. p. 269.

[7] Ricardson R, Evans B. A review of pulse tube refrigeration. Int J Refrig 1997;20:367–73.

[8] Popescu G, Radcenco V, Gargalian E, Bala P. A critical review of pulse tube cryogenerator research. Int J Refrig 2001;24:230–7.

[9] Nika P, Bailly Y. Comparison of two models of a double inlet miniature pulse tube refrigerator: Part A thermodynamics. Cryogenics 2002;42:593–603.

[10] Chen G, Gan Z, Thummes G, Heiden C. Thermodynamic performance of pulse tube refrigeration with mixture fluids. Cryogenics 2000;40:261–7.

[11] Gedeon D. Pulse tube model-class reference guide. Gedeon Associates; 1999.

[12] Ju Y, Wang C, Zhou Y. Numerical simulation and experimental verification of the oscillating flow in pulse tube refrigerator. Cryogenics 38. p. 160–76.

[13] Hozumi Y, Shiraishi M, Murakami M. Simulation of thermodynamics aspects about pulse tube refrigerator. In: Proceedings of the international cryogenics engineering conference, September 2003. p. 1500–7.

[14] Flakes B, Razani A. Modeling pulse tube cryocoolers with CFD. In: Proceedings of the international cryogenics engineering conference, September 2003. p. 1493–9.

[15] Fluent INC. Fluent 6 User Manual. Fluent INC; 2003. p. 8-1.

[16] Kirkconnell C. Numerical analysis of the mass flow and thermal behavior in high-frequency pulse tubes, PhD thesis, Georgia Institute of Technology, Atlanta, GA, 1995.

[17] Kirkconnell C, Soloski S, Price K. Experiments on the effects of pulse tube geometry on PTR performance. Cryocoolers 1997;9:285.

[18] Harvey J, Kirkconnell C, Desai P. Comparison of entropy generation rates in various stirling-class cryocooler configurations. In: Proceedings of the international cryogenics engineering conference, September 2003. p. 1519–26.

[19] Harvey J. Parametric study of cryocooler regenerator performance, MS Thesis, Georgia Institute of Technology, Atlanta, GA, 1999.

[20] Cooper W, Nee V, Yang K. An experimental investigation of convective heat transfer from the heated floor of a rectangular duct to a low frequency, large tidal displacement oscillatory flow. Int J Heat Mass Trans 1994;37:581–92.

[21] Zhao T, Cheng P. A numerical solution of laminar forced convection in a cheated pipe subjected to a reciprocating flow. Int J Heat Mass Transfer 1995;38:3011–22.

[22] Moschandreou T, Zamir M. Heat transfer in a tube with pulsating flow and constant heat flux. Int J Heat Mass Transfer 1997;40:2461–6.

[23] Li P, Yang K. Mechanisms for the heat transfer enhancement in zero-mean oscillatory flows in short channels. Int J Heat Mass Transfer 2000;43:3551–66.

[24] Sert C, Beskok A. Numerical simulation of reciprocating flow forced convection in two-dimensional channels. ASME Trans J Heat Tran 2003;125:403–12.

[25] Mark A, Koning C, Hamersma P, Fortuin J. Axial dispersion in single phase flow in a porous packed column containing structured packing. Chem Eng Sci 1991;46:819–26.

[26] Mark A, Hamersma P, Fortuin J. Solid hold up and axial dispersion during counter current solid-liquid contacting in a pulsed packed column containing structured packing. Chem Eng Sci 1992;47:565–77.

[27] Crittenden B, Field R, Pervez M. Oscillatory flow in packed beds and baffled tubes. A unifying approach to the interpretation of experimental data. Chem Eng Sci 1995;50:3839–45.

[28] Lau A, Crittenden B, Field R. Enhancement of liquid phase absorption column performance by means of oscillatory flow: an experimental study. Separation Purifi Technol 2004;35:113–24.

[29] Zhao T, Cheng P. Oscillatory pressure drops through a woven-screen packed column subjected to a cyclic flow. Cryogenics 1996;36:333–41.